

Proposal for a photoelectron spectroscopy and microscopy beamline (0.5–11 keV) at the High Energy Photon Source

Kun Tang,* Lei Zheng, Jia-Ou Wang and Yi-Dong Zhao

Institute of High Energy Physics, 19B Yuquan Road, Shijingshan District, Beijing, People's Republic of China.

*Correspondence e-mail: tangk@ihep.ac.cn

Received 29 September 2018

Accepted 9 January 2019

Edited by I. Schlichting, Max Planck Institute for Medical Research, Germany

Keywords: PES/HAXPES; PEEM/HAXPEEM; beamline; X-ray optics.

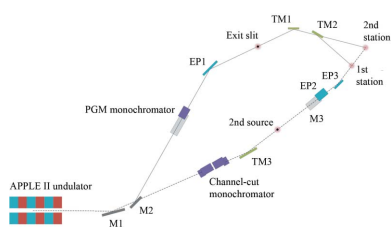
An optical design study of a beamline proposed for the new 6 GeV synchrotron, the High Energy Photon Source (HEPS), to be built in Beijing, China, is described. The beamline is designed to cover an energy range from 0.5 to 11 keV with two experimental stations, one for X-ray photoelectron spectroscopy (PES) experiments and the other for photoelectron emission microscopy (XPEEM) experiments. A 5 m APPLE II-type undulator with a relatively long magnetic period (55 mm) is used as the only radiation source. To optimize the optical efficiency for the full energy range, the beamline is split into a soft X-ray branch that is based on a variable-line-spacing plane-grating monochromator and a tender X-ray branch that uses a four-bounce monochromator with three Si channel-cut pairs. To allow both PES and XPEEM to be performed over the entire energy range, two toroidal mirrors and a bendable KB mirror pair are employed to deliver the soft and tender beams, respectively, to either of two experimental stations.

1. Introduction

The High Energy Photon Source (HEPS), a 6 GeV diffraction-limited ~ 60 pm rad storage-ring light source, is under construction in Beijing, China, and will be operational before 2025 (Jiao *et al.*, 2018). The overall planning goal of HEPS comprises more than 90 beamlines, with 14 being carried out in Phase I. This proposal does not address Phase I, but examines the future of HEPS.

X-ray photoelectron spectroscopy (XPS/PES) based on synchrotron radiation has seen tremendous growth over the past 30 years. However, XPS (<2 keV) is generally considered to be a surface-sensitive technique compared with hard X-ray photoelectron spectroscopy (HAXPES) (Yamasaki *et al.*, 2005). Higher-energy photons mean that depths of up to several tens of nanometres can be probed in a nondestructive manner (Risterucci *et al.*, 2014). A combined beamline with soft and hard X-rays could allow for variable depth analysis, making PES/HAXPES possible. A beam size of dozens of micrometres can meet most needs in PES/HAXPES and make available micro-angle-resolved PES/HAXPES (μ APRES), standing-wave PES/HAXPES (Nemšák *et al.*, 2018; Wu *et al.*, 2018) and scanning-microscope PES/HAXPES. With an adjustable polarized source (Fujiwara *et al.*, 2016; Kozina *et al.*, 2011), magnetic circular/linear dichroism (MCD/MLD) PES/HAXPES is also useful.

A photoelectron emission microscope (XPEEM/HAXPEEM) adds lateral resolution to PES/HAXPES to acquire an energy-filtered three-dimensional picture, and thus both energy resolution (~ 0.1 eV) and lateral resolution



(~50 nm) can be achieved theoretically. The lateral resolution is not limited by spot size but is mainly determined by the electron-optical properties of the immersion lens (Wiemann *et al.*, 2012; Uhlir *et al.*, 2010). However, the signal from XPEEM/HAXPEEM is much lower than that in the ultraviolet regime due to the reduced photoionization cross-section and the transmission of the instrument. To improve the signal-to-noise ratio and the statistical quality, the beam size should be comparable with the field of view of the microscope, and the flux density should not be less than 10^9 photons $s^{-1} \mu m^{-2}$ according to the experiments at PETRA III P09 (Patt *et al.*, 2014).

As of 2018, many HAXPES facilities exist in the world, such as BESSY II EMIL (Hendel *et al.*, 2016), NSLS II ID07 (Reininger *et al.*, 2011), Diamond Light Source ID09 (Lee & Duncan, 2018) and SPring-8 BL12XU, BL15XU, BL39XU, BL46XU and BL47XU (Fujiwara *et al.*, 2016; Yasuno *et al.*, 2016; Suzuki *et al.*, 2013), among others, along with several HAXPES/HAXPEEM integrated stations, such as BESSY II EMIL and NSLS II ID07, mentioned above, and PETRA III P09 (Gloskovskii *et al.*, 2012) or P22, and SOLEIL GALAXIES (Rueff *et al.*, 2015). Some of them are two-colour beamlines allowing soft and hard X-rays on the same sample at the same time, such as two well known beamlines Diamond Light Source ID09 and NSLS II ID07.

According to the scientific contributions of similar beamlines around the world, a beamline with an energy range from 0.5 to 11 keV with micrometre beam size and high flux to 10^{10} photons $s^{-1} \mu m^{-2}$ with an adjustable polarized source could make most of the experimental techniques based on PES/HAXPES available. In the sections below we describe the beamline and the expected performance.

2. Insertion devices

An advanced planar polarized light emitter (APPLE II) type undulator with a magnetic period of 55 mm, a total length of 5.0 m and a minimum gap of approximately 11 mm will provide soft X rays with variable polarization in the range 500–2200 eV and tender X rays of up to 11 keV with horizontal or vertical linear polarized radiation. Insertion of similar specifications (Viefhaus *et al.*, 2013) has been utilized in PETRA III XUV beamline P04. There are reasons for choosing only one APPLE II undulator, such as limited space for a canted beamline and vertical polarization for a tender branch beamline.

Under the condition of horizontal polarized radiation, the source size and divergence in the horizontal and vertical directions are calculated and the results are listed in Table 1. These calculations were performed using the *SPECTRA* code (Tanaka & Kitamura, 2001).

The receiving aperture is approximately $50 \mu rad \times 60 \mu rad$ in the soft branch and approximately $30 \mu rad \times 30 \mu rad$ in the

Table 1
Source size and divergence in the horizontal and vertical directions.

		Source size, 1σ (μm)		Source divergence, 1σ (μrad)	
		Horizontal	Vertical	Horizontal	Vertical
First harmonic	0.5 keV	13.5	13.2	18.2	16.7
	1 keV	10	9.8	13.8	11.9
	2 keV	7.9	7.5	10.9	8.4
	5 keV	6.2	5.7	8.8	5.4
Third harmonic	5 keV	6.2	5.7	9.8	7
	10 keV	5.5	5	8.5	5

tender branch. The horizontal polarized flux emitted by the devices integrated over the central cone performed with the *SPECTRA* code is shown in Fig. 1, assuming a ring current of 200 mA.

3. Optical layout

To optimize the optical efficiency for the full energy range, the beamline is split into a soft X-ray branch (0.5–2.2 keV) that is based on a variable-line-spacing plane-grating monochromator (PGM) and a tender X-ray branch (2.1–11 keV) that uses a high-resolution monochromator (HRM) with channel cuts. A total of nine mirrors, including three flat mirrors (M1, M2, M3), three elliptical cylinder mirrors (EP1, EP2, EP3) and three toroidal mirrors (TM1, TM2, TM3) are used for optics. A top-view schematic of the beamline is shown in Fig. 2.

The thermal load of a soft beamline is always a fatal problem, especially in a high-energy ring. We deal with this problem using two heat-load-absorption mirrors. The upstream mirror, M1, achieves a cut-off energy of approximately 11 keV, and is shared by the two branches. The beam transmission direction could be transformed depending on the status of the downstream mirror, M2. Mirror M2 will be used in the soft branch to cut off the excess power above 2.2 keV, but not used in the tender branch. In the worst case, the maximum thermal loads absorbed by M1 and M2 are approximately 600 and 90 W, respectively, with maximum

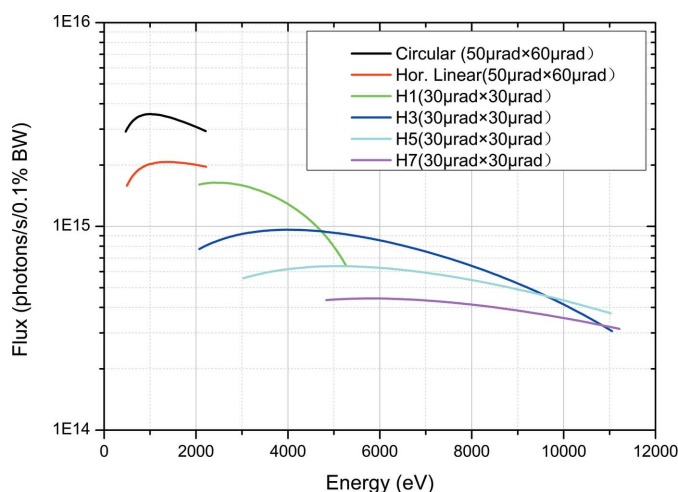


Figure 1
Characteristics of APPLE II UE55.

Table 2
Optical parameters of the soft and tender branches.

Parameters of M1 in the soft branch are omitted, but are shown in the tender branch. RMS denotes root mean square. Hor denotes horizontal.

Soft branch	M2	PM	PG	EP1	TM1	TM2
Distance (m)	43	~59.8	~60	72	85	85.5
Reflection direction	Hor +	Upwards	Downwards	Hor –	Hor –	Hor –
Final shape	Flat	Flat	Flat	Elliptical	Toroidal	Toroidal
Tangential bending	–	–	–	Yes	–	–
Object distance (m)	–	–	60	72	5	–6.5
Image distance (m)	–	–	20	8	7	4.5
Tangential radius (m)	–	–	–	~816	393	1970
Sagittal radius (m)	–	–	–	–	0.0865	0.44
Dimensions (L × W × H) (mm)	180 × 60 × 100	450 × 40 × 60	200 × 40 × 30	200 × 60 × 10	200 × 40 × 30	200 × 40 × 30
Angle of incidence	0.8°	1.5°–3.3°	0.8°–1.8°	1.2°	0.85°	0.85°
Coating	B ₄ C	Au	Au	Au	Au	Au
Roughness (nm RMS)	<0.3	<0.2	<0.15	<0.2	<0.3	<0.3
Material	Silicon	Silicon	Silicon	Silicon	Silicon	Silicon
Slope error (μrad RMS)	0.5/5	0.2/3	0.15/3	0.2/3	0.3/5	0.3/5

Tender branch	M1	HRM	TM3	M3	EP2	EP3
Distance (m)	40	64	68	86.2	87.5	88
Reflection direction	Hor +	–	Hor +	Upwards	Downwards	Hor +
Final shape	Flat	Flat	Toroidal	Flat	Elliptical	Elliptical
Tangential bending	–	–	Yes	–	Yes	Yes
Object distance (m)	–	–	68	–	7.5	7.8
Image distance (m)	–	–	12	–	~2.5/4.5	~2.2/4.2
Tangential radius (m)	–	–	3520	–	~647/970	~592/941
Sagittal radius (m)	–	–	0.1183	–	–	–
Dimensions (L × W × H) (mm)	750 × 60 × 100	–	380 × 60 × 40	220 × 40 × 30	240 × 40 × 10	240 × 40 × 10
Angle of incidence (mrad)	2.8	16–75°	5.8	5.8	5.8	5.8
Coating	B ₄ C	–	B ₄ C/Pt	B ₄ C, Pt	B ₄ C, B ₄ C/Pt	B ₄ C/Pt
Roughness (nm RMS)	<0.3	<0.3	<0.2	<0.2	<0.2	<0.2
Material	Silicon	Silicon	Silicon	Silicon	Silicon	Silicon
Slope error (μrad RMS)	0.5/5	–	0.3/5	0.2/3	0.2/3	0.2/3

power densities of <0.35 and $<0.25 \text{ W mm}^{-2}$, respectively. The results of finite-element-method analysis indicate that a smart-cut design with a top-side cooling scheme could handle such heat loads of both mirrors, achieving acceptable slope error. After two rounds of heat absorption, the remaining maximum power will be under 30 W such that the power densities of both PM and PG are less than 0.1 W mm^{-2} at worst. In the tender branch, under the additional limitation of an aperture of $30 \mu\text{rad} \times 30 \mu\text{rad}$ after M1, the remaining maximum power

imposed on the crystal is less than 40 W and the maximum power density of the spot cross-section is $<10 \text{ W mm}^{-2}$. Such a heat load could be easily handled by liquid-nitrogen cooling. The optical parameters of the two branches are listed in Table 2.

Under the optical parameters in Table 2, ideally two branches could be focused to either of the experimental stations at the same point. Furthermore, adjustment with independent degrees of freedom, including horizontal and vertical, and focusing are important and could enable this design practically. First, the horizontal degree of freedom is realized by the fine tuning of the reflection angles of M2 and EP3. Second, the vertical degree of freedom is realized by adjusting the position and reflection angle of M3. HRM will not change the lateral position or transmission direction of the beam, which is reflected upwards by M3 and downwards by EP2 in the vertical direction. The height increase of the M3–EP2 combination is approximately 15 mm, which is equal to that of the PGM in the soft branch. The distance between M3 and EP2 should be approximately 1293 mm, while the reflection angle for both mirrors is

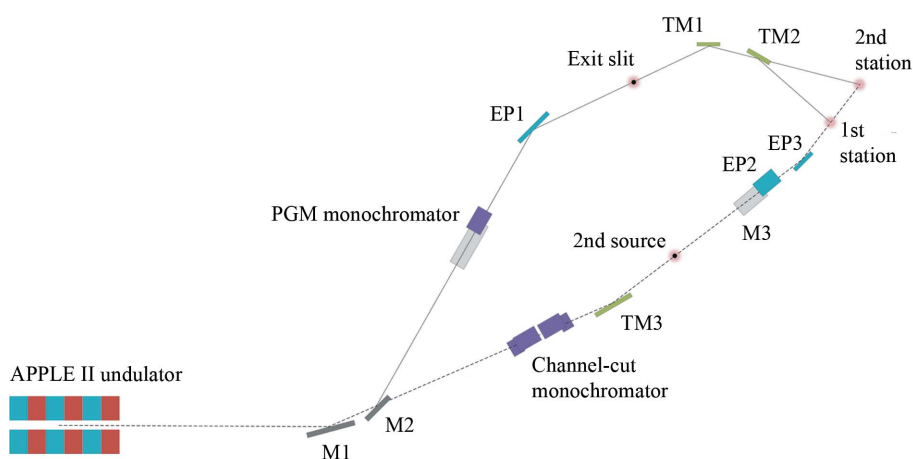


Figure 2
Top view of the beamline optical layout.

Table 3
Optical parameters of PGM gratings.

Grating parameters	HEG	LEG
Groove density (lines mm ⁻¹)	1200	600
Ruled area (L × W) (mm)	180 × 15	180 × 15
<i>cla</i>	0.65	0.55
Groove depth (nm)	4.0	6.5
VLS parameters		
<i>a</i> 0 (mm ⁻¹)	1200	600
<i>a</i> 1 (mm ⁻²)	0.144	0.084
<i>a</i> 2 (mm ⁻³)	1.0 × 10 ⁻⁵	5.7 × 10 ⁻⁵

approximately 5.8 mrad. Finally, the focusing degree of freedom is realized by bending EP2 and EP3.

Space between the two branches for the installation of the different optical components, particularly for those close to the experimental stations, is also an important issue. Thus, all the optical components of each branch are staggered as far as possible in the direction of beam propagation in this design. At the position of the KB mirror pair, the lateral distance between each branch is approximately 300 mm and the intersection angle is approximately 125 mrad, which seems to be sufficient. The lateral distance between the two branches is approximately 475 mm at the PGM position and approximately 588 mm at the HRM position. The spaces are not larger, but are already sufficient. Moreover, the lateral space problems of one branch could be solved by light passing through the vacuum cavity of another branch if the lateral space is not sufficient as engineered.

3.1. Expected energy resolution

The monochromator of the soft branch will be a PGM with variable-line-spacing (VLS) gratings. The monochromator will be equipped with two gratings with line densities of 600 lines mm⁻¹ (LEG) and 1200 lines mm⁻¹ (HEG) at their centers and operated with *c*_{ff} values of 2.08 and 2.76, respectively, one for flux and the other for energy resolution. The optical parameters of the gratings are listed in Table 3.

The monochromator of the tender branch will not use a conventional double-crystal monochromator (DCM) but rather a high-resolution double-channel-cut (four-bounce) monochromator directly. Research (Hayama *et al.*, 2018) has shown that very high quality channel-cut crystals can be produced, which demonstrate excellent performance in liquid-nitrogen-cooled monochromators. To cover the entire range of 2.1–11 keV with an energy resolution of 100–400 meV, three Si channel-cut pairs, Si(111), Si(220) and Si(311), are used with symmetric reflections. The channel-cut angles range from 16° to 75°, so as to achieve the following energy ranges, 2.05–7.1 keV, 3.35–11.6 keV and 3.9–13.6 keV, respectively.

Under the linear polarized radiation of the source, the expected resolution of each branch is calculated as shown in Fig. 3. The calculation takes into account the influence of the surface error, as shown in Table 1. We also select some energy points with the horizontal polarization source for verification using *Shadow/XOP* software (Canestrari *et al.*, 2011),

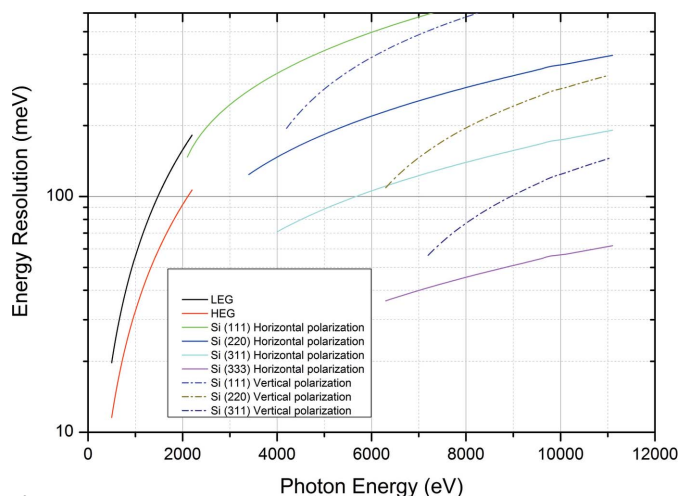


Figure 3
Energy bandwidths of different monochromator configurations. The grating monochromator uses a 10 μm exit slit, and the crystal monochromator uses a double-channel-cut with (+ – +) configuration (zero offset). All of the analysis presented in Section 3 is based on these parameters.

including the results, for example, 32 meV at 1 keV with HEG, 150 meV at 2.5 keV with Si(111), 185 meV at 5 keV with Si(220), and 200 meV at 10 keV with Si(311).

3.2. Expected focus

In the soft branch, all of the following mirrors deflect the beam in the horizontal direction. EP1 transfers the source to the exit slit with a horizontal demagnification of approximately 9:1, TM1 is the refocusing mirror that achieves the focus of the second station at approximately 92 m, and TM2 plays the role of an additional refocusing mirror that is toroid shaped. Combining TM1 and TM2, the refocus position is able to be shifted to the first station at 90 m. The full width at half-maximum (FWHM) at each station is 30 μm × 10 μm and 43 μm × 14 μm, respectively. The upstream focal spot is smaller.

In the tender branch, TM3 deflects the beam in the horizontal direction, focusing the source along both the horizontal and vertical directions with a demagnification of approximately 5.67:1, generating a secondary source. The FWHM of the secondary source is approximately 23 μm × 5 μm, mainly due to the slope error and aberration of optics. A KB system of elliptical cylinders (EP2 and EP3) refocuses the above secondary source in both the vertical and horizontal directions, respectively. The final beam spot size could be detuned using the bender of the KB. Under the condition of focusing, the FWHMs at each station are 7 μm × 5 μm and 13 μm × 8 μm, respectively. All the simulation calculations take surface error into account and are performed with the *Shadow/XOP* code.

3.3. Expected flux with polarization

The optical efficiencies of both branches are shown in Fig. 4. The reflectivity of the mirrors with fixed grazing incidence is calculated using *XOP*. The scalar theory efficiency of a

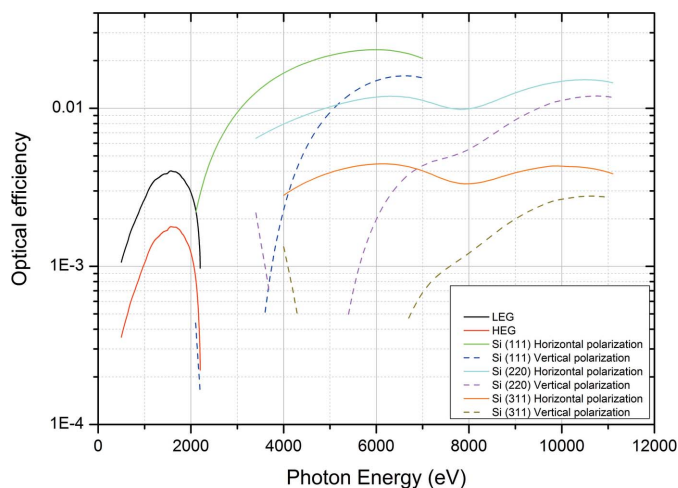


Figure 4
Optical efficiencies as a function of photon energy leading to focus.

laminar grating with duty ratio $c/a = 0.5$ is given by a formula included in the CXRO X-ray booklet, and we derived an expansion version with different duty ratio for preliminary estimation. Fundamental optical parameters, such as mirrors and crystals, are generated by *XOP DABX*. The calculation considers the effect of the transmission bandwidth, changing the units from photons s^{-1} (0.1% bandwidth) $^{-1}$ to photons s^{-1} .

In the tender branch, horizontal and vertical polarizations based on an APPLE II source are used, and the flux of vertical polarization at a station will be less than that of horizontal polarization. The orthogonal linear polarization could be useful over almost the entire range between 2.1 and 11 keV, which is not easily implement with a phase retarder. However, a phase retarder (Fujiwara *et al.*, 2016) is still needed to generate circular polarization. The circularly polarized or linear horizontally polarized flux expected at an experimental station is shown in Fig. 5.

3.4. Harmonic suppression

In the soft branch (<2.2 keV), the ratio of the higher harmonic is less than 1% in the worst case, calculated as the number of photons. However, the calculation results are based on the reflectivity of the mirrors and a scalar estimate by the formula of grating efficiency; further optical simulation verification would be required if desired in the future.

In the tender branch (>2.1 keV), M3 is a harmonic suppression mirror with two coatings. The B_4C coatings effectively cut off the energy above 5.5 keV, achieving a suppression ratio of the harmonic of approximately 10 at 2.1 keV. Such a harmonic suppression ratio seems to be insufficient in some experiments in which EP2 plays the role of another harmonic mirror realized by the B_4C coating. The ratio of the higher harmonic could be controlled under the level of 1%. However, composite coatings (15 nm B_4C on 30 nm Pt) of EP2 could smooth the reflection curve and are conventionally used in the energy range 2.5–11 keV.

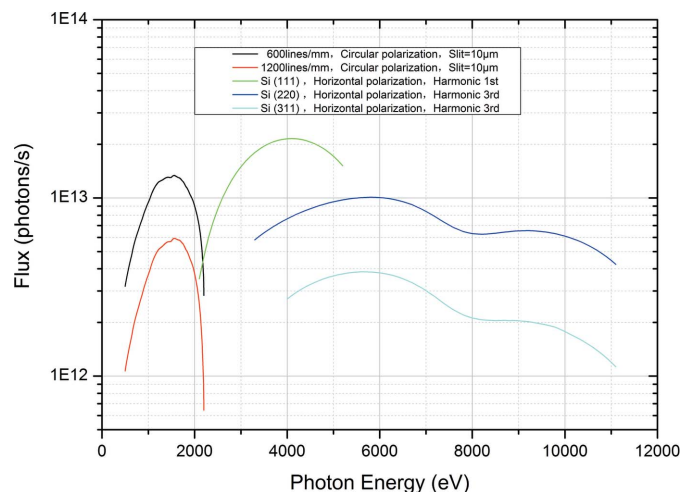


Figure 5
Expected flux at the endstation.

4. Conclusions

We have described a proposed beamline for HEPS, a beamline that will have two experimental stations, one for PES/HAXPES experiments and another for PEEM/HAXPEEM experiments, both in the energy range 0.5–11 keV on the same sample. This beamline could provide a nondestructive and depth-selective measurement of electronic structure, chemistry and bond orientation. With the construction of HEPS, additional proposals will be the objects of discussion in the next several years.

Acknowledgements

We thank LetPub (<http://www.letpub.com>) for its linguistic assistance during the preparation of this manuscript.

References

- Canestrari, N., Karkoulis, D. & Sánchez del Río, M. (2011). *Proc. SPIE*, **8141**, 814112.
- Fujiwara, H., Naimen, S., Higashiya, A., Kanai, Y., Yomosa, H., Yamagami, K., Kiss, T., Kadono, T., Imada, S., Yamasaki, A., Takase, K., Otsuka, S., Shimizu, T., Shingubara, S., Suga, S., Yabashi, M., Tamasaku, K., Ishikawa, T. & Sekiyama, A. (2016). *J. Synchrotron Rad.* **23**, 735–742.
- Gloskovskii, A., Stryganyuk, G., Fecher, G. H., Felser, C., Thiess, S., Schulz-Ritter, H., Drube, W., Berner, G., Sing, M., Claessen, R. & Yamamoto, M. (2012). *J. Electron Spectrosc. Relat. Phenom.* **185**, 47–52.
- Hayama, S., Duller, G., Sutter, J. P., Amboage, M., Boada, R., Freeman, A., Keenan, L., Nutter, B., Cahill, L., Leicester, P., Kemp, B., Rubies, N. & Diaz-Moreno, S. (2018). *J. Synchrotron Rad.* **25**, 1556–1564.
- Hendel, S., Schäfers, F., Hävecker, M., Reichardt, G., Scheer, M., Bahrdt, J. & Lips, K. (2016). *AIP Conf. Proc.* **1741**, 030038.
- Jiao, Y., Xu, G., Cui, X.-H., Duan, Z., Guo, Y.-Y., He, P., Ji, D.-H., Li, J.-Y., Li, X.-Y., Meng, C., Peng, Y.-M., Tian, S.-K., Wang, J.-Q., Wang, N., Wei, Y.-Y., Xu, H.-S., Yan, F., Yu, C.-H., Zhao, Y.-L. & Qin, Q. (2018). *J. Synchrotron Rad.* **25**, 1611–1618.
- Kozina, X., Fecher, G. H., Stryganyuk, G., Ouardi, S., Balke, B., Felser, C., Schönhense, G., Ikenaga, E., Sugiyama, T., Kawamura, N., Suzuki, M., Taira, T., Uemura, T., Yamamoto, M., Sukegawa, H., Wang, W., Inomata, K. & Kobayashi, K. (2011). *Phys. Rev. B*, **84**, 054449.

- Lee, T. L. & Duncan, D. A. (2018). *Synchrotron Radiat. News*, **31**(4), 16–22.
- Nemšák, S., Gehlmann, M., Kuo, C. T., Lin, S. C., Schlueter, C., Mlynczak, E., Lee, T. L., Plucinski, L., Ebert, H., Di Marco, I., Minár, J., Schneider, C. M. & Fadley, C. S. (2018). *Nat. Commun.* **9**, 3306.
- Patt, M., Wiemann, C., Weber, N., Escher, M., Gloskovskii, A., Drube, W., Merkel, M. & Schneider, C. M. (2014). *Rev. Sci. Instrum.* **85**, 113704.
- Reininger, R., Woicik, J. C., Hulbert, S. L. & Fischer, D. A. (2011). *Nucl. Instrum. Methods Phys. Res. A*, **649**, 49–51.
- Risterucci, P., Renault, O., Martinez, E., Detlefs, B., Delaye, V., Zegenhagen, J., Gaumer, C., Grenet, G. & Tougaard, S. (2014). *Appl. Phys. Lett.* **104**, 051608.
- Rueff, J.-P., Ablett, J. M., Céolin, D., Prieur, D., Moreno, T., Balédent, V., Lassalle-Kaiser, B., Rault, J. E., Simon, M. & Shukla, A. (2015). *J. Synchrotron Rad.* **22**, 175–179.
- Suzuki, M., Kawamura, N., Mizumaki, M., Terada, Y., Uruga, T., Fujiwara, A., Yamazaki, H., Yumoto, H., Koyama, T., Senba, Y., Takeuchi, T., Ohashi, H., Nariyama, N., Takeshita, K., Kimura, H., Matsushita, T., Furukawa, Y., Ohata, T., Kondo, Y., Ariake, J., Richter, J., Fons, P., Sekizawa, O., Ishiguro, N., Tada, M., Goto, S., Yamamoto, M., Takata, M. & Ishikawa, T. (2013). *J. Phys. Conf. Ser.* **430**, 012017.
- Tanaka, T. & Kitamura, H. (2001). *J. Synchrotron Rad.* **8**, 1221–1228.
- Uhlíř, V., Pizzini, S., Rougemaille, N., Novotný, J., Cros, V., Jiménez, E., Faini, G., Heyne, L., Sirotti, F., Tieg, C., Bendounan, A., Maccherozzi, F., Belkhou, R., Grollier, J., Anane, A. & Vogel, J. (2010). *Phys. Rev. B*, **81**, 224418.
- Viefhaus, J., Scholz, F., Deinert, S., Glaser, L., Ilchen, M., Seltmann, J., Walter, P. & Siewert, F. (2013). *Nucl. Instrum. Methods Phys. Res. A*, **710**, 151–154.
- Wiemann, C., Patt, M., Cramm, S., Escher, M., Merkel, M., Gloskovskii, A., Thiess, S., Drube, W. & Schneider, C. M. (2012). *Appl. Phys. Lett.* **100**, 223106.
- Wu, M.-Y., Huang, Q.-S., Le Guen, K., Ilakovac, V., Li, B.-X., Wang, Z.-S., Giglia, A., Rueff, J.-P. & Jonnard, P. (2018). *J. Synchrotron Rad.* **25**, 1417–1424.
- Yamasaki, A., Sekiyama, A., Imada, S., Tsunekawa, M., Higashiya, A., Shigemoto, A. & Suga, S. (2005). *Nucl. Instrum. Methods Phys. Res. A*, **547**, 136–150.
- Yasuno, S., Oji, H., Koganezawa, T. & Watanabe, T. (2016). *AIP Conf. Proc.* **1741**, 030020.